DESIGNED MONOMERS AND POLYMERS
2021, VOL. 24, NO. 1, 162–172
https://doi.org/10.1080/15685551.2021.1930670

Taylor & Francis
Taylor & Francis Group

The surface morphology and dynamic impact properties with rebounding and splashing of water droplet on phase separation and breath figure assisted electrospinning films

Que Kong[a], Zhiguang Li[a], Xuehong Ren[a], Hao Gu[b] and Wujun Ma[c]

[a]Key Laboratory of Eco-textiles of Ministry of Education, College of Textile Science and Engineering, Jiangnan University, Wuxi, China; [b]The technology department, Shinefair Special Materials Co., Ltd, Huzhou, China; [c]College of Textile and Garment, Nantong University, Nantong, China

ABSTRACT

Electrospinning provides a versatile, efficient and low-cost method for the preparation of continuous nanofibres from various polymers. In this study, the polyhedral oligomeric silsesquioxanes (POSS) block copolymer was synthesized via atom transfer radical polymerization. The smooth fiber, porous fiber or hierarchically porous microspheres were prepared by electrospinning from POSS block copolymer, poly(vinylidene fluoride) (PVDF) and aluminium oxide (Al_2O_3). The influence of copolymer concentration, the ratio of the solvents, the diameter and concentration of the Al_2O_3 on the surface morphology were investigated. Porous fibers and porous microspheres were prepared by regulating the ratio of the solvents from the phase separation and breath figure methods. The dynamic behavior of the water droplet with the constant volume impacting on the electrospinning films were reported. The morphology evolution, restitution coefficient, the change of energy of the water droplets are examined. The droplet bounces several times on the superhydrophobic surface, while the droplet remains pinned and does not rebound when the contact angles was lower than 150°. On the other hand, the water droplets were splashed on the Al_2O_3 based electrospinning films. Finally, the mechanical properties of the electrospinning films were investigated.

ARTICLE HISTORY
Received 19 March 2021
Accepted 12 May 2021

KEYWORDS
Electrospinning films; breath figure; splashing; dynamic impact properties; superhydrophobicity

1. Introduction

Superhydrophobicity surface with water contact angle over 150° implying extreme water repellency which can be used in many industrial applications, such as self-cleaning, antifouling, and functional textiles[1]. However, the preparing methods of superhydrophobicity surface have some disadvantages, for example, the relatively complicated production equipments [2,3], the expensive price of the materials [4] and the complexity of the method[5]. Thus, preparing a controllable hydrophobic surface with efficient, inexpensive price, and convenient method is still a challenge[6]. Electrospinning is a simple, effective and straightforward procedure to generate micro/nanofibers with hydrophobic property [7–11]. Pores, beads can be prepared on the fiber surface or composite fibers in order to increase the surface hydrophobic property [12–14].

The impact dynamics of droplets on surfaces plays an important role in some procedures, including coffee splitting, dropwise condensation, anti-icing and self-cleaning. The dynamic droplet impact action is an effective method to characterize the surface property [15,16]. The superhydrophobicity is increased by surface roughness and low surface energy, which can be understood and controlled through drop impact behavior[17]. The droplet can exhibit sticking, spreading, bouncing, or pinning when collides with a solid surface [18,19]. The state of the water droplet is varied according to the liquid-solid interaction and are influenced by the droplet's velocity, density and viscosity [20–22]. In addition, the roughness and surface energy of substrates will also affect the impact behaviors significantly. Droplet impact behavior leads to a general sketch of time evolution. Moreover, the adhesion of the droplet is extraordinary significance which determines the dynamic behavior of the droplet. In brief, the roughness structure and chemical composition also influence the adhesive property of the surface [23,24], which could be adjusted to obtain controlled adhesion.

Polyhedral oligomeric silsesquioxanes (POSS) based fluorine block copolymer is an organic-inorganic hybrid material. In addition, it has an inorganic core can reduce the surface energy of the material and

CONTACT Zhiguang Li lizg@jiangnan.edu.cn; Xuehong Ren xhren@jiangnan.edu.cn Key Laboratory of Eco-textiles of Ministry of Education, College of Textile Science and Engineering, Jiangnan University, Wuxi 214122, China

therefore has good performance in terms of hydrophobicity [25,26]. On the other hand, polyvinylidene fluorid (PVDF) has low surface energy (30.3×10^3 N/m) which can be used in electrospinning to obtain hydrophobic electrospun membrane, and the contact angle is approximately 120–130° [27,28]. Al_2O_3 is a micro-nano sphere which can enhance the surface roughness [29,30]. As a result, it can render surface hydrophobic property.

In this paper, the POSS block copolymer, PVDF and Al_2O_3 nanoparticles as spinning fluid composition, DMF and THF as mixed solvents, were prepared by electrospinning technology to obtain superhydrophobic surfaces. The concentration of block copolymer, the ratio of the DMF and THF, the concentration of the Al_2O_3 were regulated. The surface morphologies and contact angles of the electrospinning films were examined. Furthermore, the dynamic properties of the electrospinning films was also investigated. The morphology variation, restitution coefficient, and energy conversion of the water droplets were studied. The mechanical properties of the electrospinning films were investigated.

2. Experimental section

2.1 Materials

PVDF was obtained from Dongguan xuanyang plastic material company ($M_n = 8 \times 10^5$ g/mol). Deionized water was purified with an ELGA Lab water system. Cuprous chloride (CuCl), tirfluoroethyl methacrylate (TFEMA), γ-Chloropropyl trimethoxysilane, pentamethyldiethylenetriamine (PMDETA) and Al_2O_3 nanoparticles are obtained from Aldrich. Methanol, Tetrahydrofuran (THF), N,N-Dimethylformamide (DMF) were obtained from Sinopharm Chemical Reagent.

2.2 Synthesis of the POSS block copolymer

The star-shaped copolymer POSS-$(PTFEMA)_8$ was synthesized through atom transfer radical polymerization[31]. The synthesis route of the POSS block copolymer is shown in Figure 1(a). The first step as follow: γ-Chloropropyl trimethoxysilane was hydrolyzed with concentrated hydrochloric acid in methanol solution at 65°C under stirring. After 5 days, the POSS-$(Cl)_8$ was obtained through washed with methanol and dried under vacuum

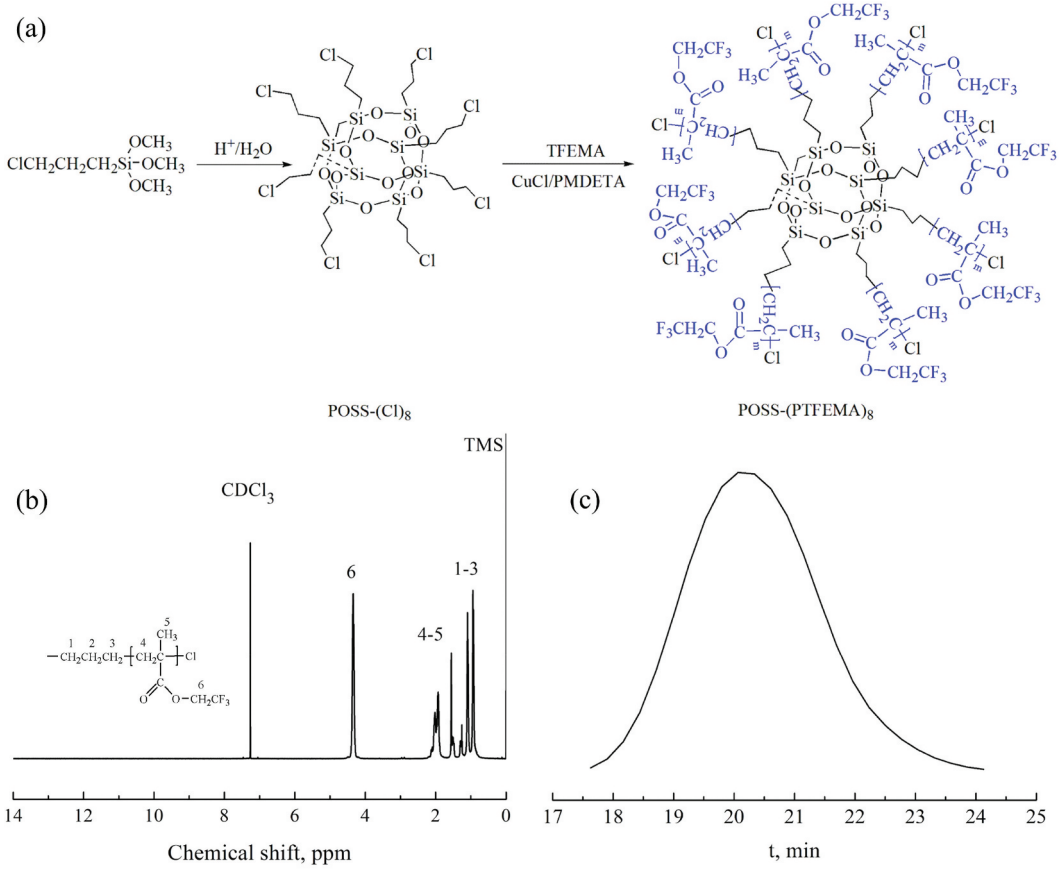

Figure 1. (a) The synthesis route, (b) ^{1}H NMR spectrum and (c) GPC trace of the POSS block copolymer.

until constant weight. The second step: POSS-$(Cl)_8$, PMDETA, TFEMA and CuCl and toluene were added into the flask by certain proportion to synthesis at 100°C without oxygen atmosphere. After 24 h, the reaction was terminated. The solution was diluted with THF, filtered over an alumina column to remove the copper salt. The product was obtained after precipitate with methanol–water solution and dried in a vacuum overnight.

The ^{1}H NMR characterization is shown in Figure 1(b). ^{1}H (500 MHz, $CDCl_3$), δ: 4.34 (s, 16 H), 2.38–1.67 (m, 16 H), 1.67–1.45 (m, 16 H), 1.10 (s, 16 H), 1.06–0.84 (m, 16 H). The molecular weight of the POSS block copolymer was 84,510 g/mol and the dispersity index (DI) is 1.33 in Figure 1(c).

2.3 Electrospinning

In this study, DMF was choose as the solvent, and THF was the non-solvent. For electrospinning, the solvents (DMF and THF) and polymers of (POSS-$(PTFEMA)_8$ and PVDF were mixed with a certain ratio. The prepared solution was subjected to magnetic stirring for 2 h. The polymer solution was loaded in a syringe connected with a metallic needle. The electrosprayed membrane were collected in a grounded aluminum foil (the distance was 12 cm). The voltage and the flowing rate were 12 kV and 1 mL/h, respectively. The electrospinning films of surface-1 to surface-8, the addition of Al_2O_3 electrospinning films of surface-9 to surface-14 are listed in Table 1 and Table 2.

2.4 Characterization

Surface morphologies of the electrospinning membranes were examined by scanning electron microscope (SEM) carried on VEGA 3 LMH (Česko TESCAN) with 10 kV accelerating voltage. Water contact angle was tested ten times by the JC2000D4 Powereach Tensionmeter. A water droplet (10 μL) at a height of 20 mm was allowed to impact on the electrospinning films. The beginning time is determined by the droplet contact with the surface. The high-speed camera (Trouble Shooter HR) records the impact behavior. The mechanical properties of the electrospinning films were determined by using a universal tensile tester (Instron 3342) with 50-N capacity load cell. The upper clamp was raised at the speed rate of 20 mm/min up to the rupture of specimens. The dimensions of test films were 50 mm × 20 mm.

3. Results and discussion

3.1 The morphologies and hydrophobic properties of the electrospinning films

The SEM images of electrospinning films from surface-1 to surface-4 are shown in Figure 2. The composition from surface-1 to surface-4 are exhibited in Table 1, as the content of PTFEMA increased, the diameter of the fabric becomes smaller and uniform. The increased polymer concentration/solution viscosity were dominated by surface tension effects and thick fibers are consequently produced[32].

When the solvents are DMF and THF, the surface morphologies are obviously changed in Figure 3. When the DMF:THF<5:5 as shown in Figure 2(c) and Figure 3 (a) and (b), the surface is very smooth without evident pore formation, and the diameter of the fabric is increased with the decrease of the DMF/THF ratio. When the DMF:THF>5:5, the porous pores are exhibited in the fiber on surface-7 and some microsphere are appeared in the film on surface-8.

Table 1. The composition of surface-1 to surface-8 via electrospinning.

Surfaces	1	2	3	4	5	6	7	8
POSS-$(PTFEMA)_8$	0 wt%	2.5 wt%	5 wt%	7.5 wt%	5 wt%	5 wt%	5 wt%	5 wt%
PVDF	15 wt%	15 wt%	15 wt%	15 wt%	15 wt%	15 wt%	15 wt%	15 wt%
DMF:THF (w/w)	10:0	10:0	10:0	10:0	8:2	5:5	2:8	1:9

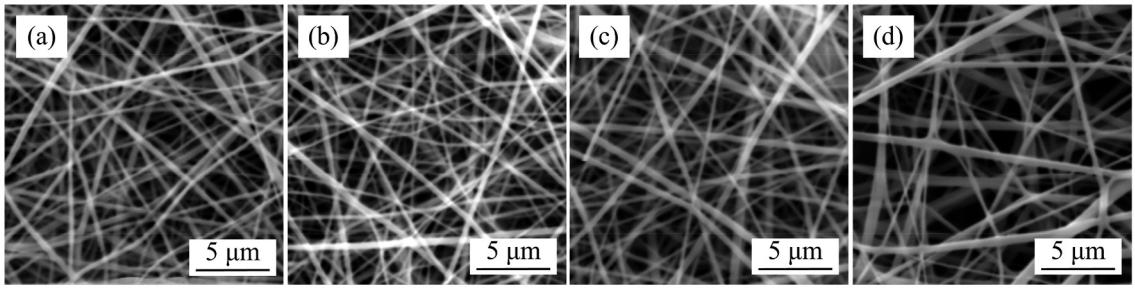

Figure 2. The SEM images of electrospinning films. (a)-(d) surface-1 to surface-4.

Table 2. The composition of surface-9 to surface-14 via electrospinning.

Surfaces	9	10	11	12	13	14
$POSS\text{-}(PTFEMA)_8$	5 wt%	5 wt%	5 wt%	5 wt%	5 wt%	5 wt%
PVDF	15 wt%	15 wt%	15 wt%	15 wt%	15 wt%	15 wt%
DMF:THF (w/w)	10:0	10:0	2:8	2:8	1:9	1:9
Al_2O_3 200 nm	5 wt%	0	5 wt%	0	5 wt%	0
Al_2O_3 20 nm	0	5 wt%	0	5 wt%	0	5 wt%

Table 3. The water contact angles of the electrospinning films.

Surfaces	CAs/°	Surfaces	CAs/°
Surfaces-1	136.1 ± 1.2	Surfaces-5	145.6 ± 1.1
Surfaces-2	141.2 ± 1.5	Surfaces-6	146.9 ± 1.3
Surfaces-3	144.8 ± 0.7	Surfaces-7	148.5 ± 1.0
Surfaces-4	148.6 ± 1.0	Surfaces-8	158.4 ± 0.9

When the DMF:THF>5:5, the breath figure and phase separation might be responsible for the pores on the fiber [33,34]. The evaporation of the volatile THF leads to the cooling effect. As a result, the high humidity may occur as the water vapor condenses on the surface for the breath figure mechanism. It is found that some rosary beads in Figure 3(c). As the increasing ratio of the THF, there are some microspheres in Figure 3(d).

The THF first evaporated from the copolymer solution in electrospinning, the non-solvent induced phase separation occurred. The polymer poor and rich phase are formed in this process. Polymer rich phase gradually shrank and the solid core of the microsphere formed. The polymer poor phase transferred onto the droplet surface[33]. On the other hand, penetrating water into the polymer solution jet raises the thermodynamic instability and evaporating solvent from that increases the polymer concentration of jet. Both events lead to raise viscoelastic forces[35]. Thus, the capillary instability is prevented and bead formation is suppressed [9,36]. In the meantime, the water vapor condenses on the surface which can be explained through breath figure method [34,37]. With the increased humidity, the water condensed onto the microsphere surface facilitated the phase separation and the polymers were solidified, and the honeycomb porous surface was formed. More non-solvent nuclei could be formed earlier and had more time to grow with a higher nonsolvent content which is beneficial to the nucleated droplet growth. On the contrary, when the DMF:THF = 1:9, the solubility is too low to form a stable jet, so it is easier to form spheres.

The water contact angles from surface-1 to surface-8 are exhibited in Table 3.

The contact angle is increased from surface-1 to surface-4 due to the content of fluorine are enhanced which decrease the surface energy. In addition, the contact angle is also increased from surface-5 to surface-8 because of the surface roughness is increased. When the DMF:THF>5:5, the porous structure increasing the surface roughness which is contributed to the superhydrophobicity. The porous fiber is formed by the rapid evaporation of the solvent to cause phase separation, rapid formation of a polymer-rich region and a solvent-rich region, and solidification on the collecting plate. Consequently, the multiscale roughness of the

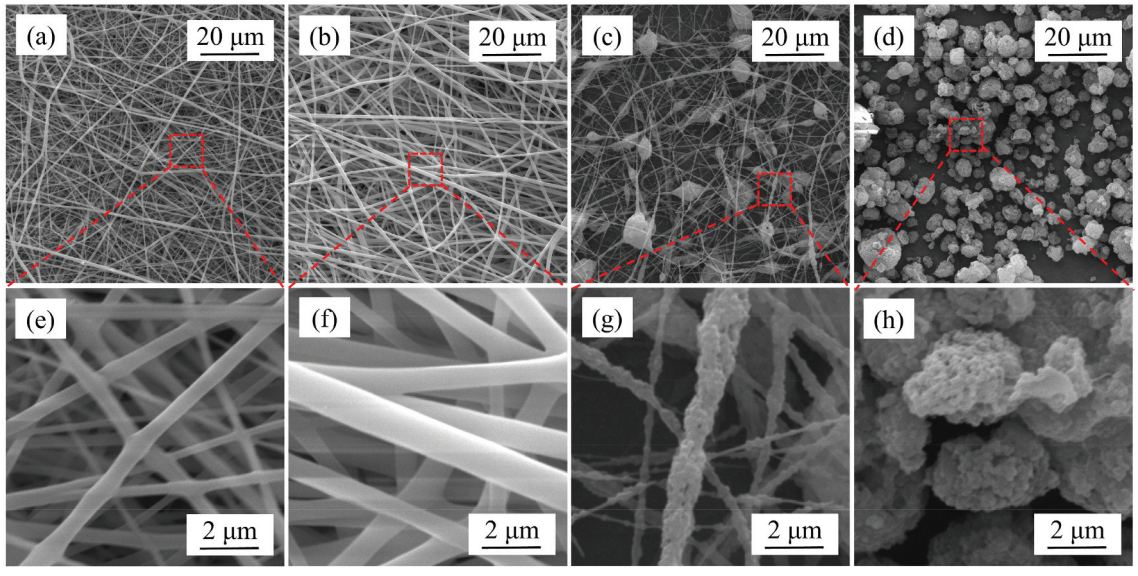

Figure 3. The SEM images of electrospinning films. (a)-(d) surface-5 to surface-8. (e)-(h) The enlargement of (a)-(d).

hierarchical structure is more than the single-scale roughness. The effect of solvents is influenced the surface structure and the hydrophobic property.

3.2 Dynamic hydrophobic properties of electrospinning films

In addition to the measurements on static water contact angle, a bouncing experiment on the electrospinning surface is conducted to further measure the hydrophobic property. The morphology evolutions of water droplets on surface-1 to surface-8 are indicated in Figure 4.

As shown in Figure 4, the morphologies of the droplets (spherical shape to pancake shape) are all the same from 0 ms to 5 ms in the eight surfaces. After 5 ms it moves back and retracts toward the center. From the 12 ms to the final state, there exist different morphologies of the water droplets on the eight surfaces. For surface-8 (Figure 4(h)), the water droplet rebounds 3 times due to its high superhydrophobic property and extremely low adhesion to water[38]. It is observed that the droplet bounces before coming to rest. The rebound is full unlike usual splashes since it may not have enough kinetic energy to fully wet the surface. The droplet has

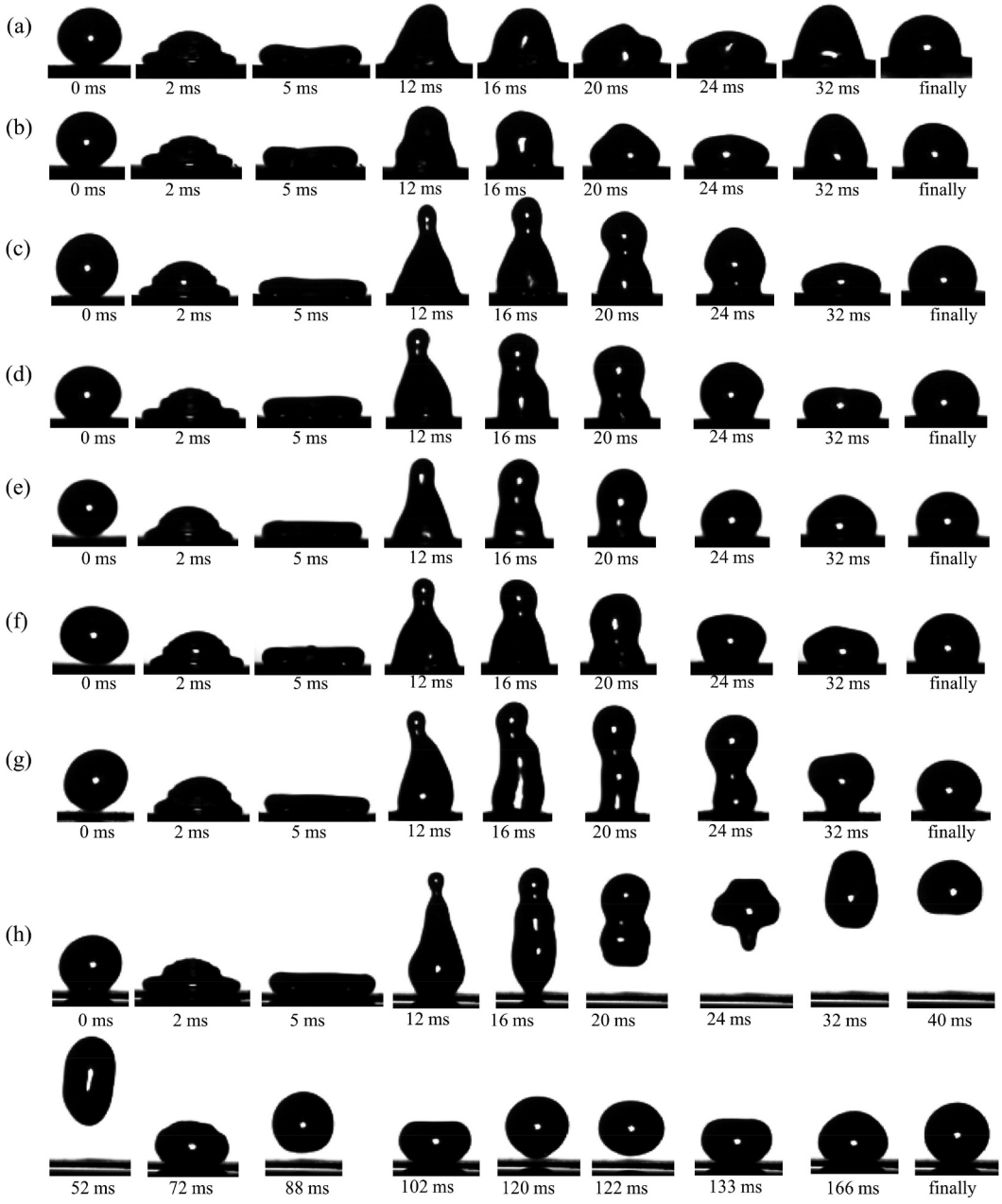

Figure 4. The morphologies of droplet impacting on different surfaces. (a)-(h) surface-1 to surface-8.

a high adhesion to water without any rebound from surface-1 to surface-7[39].

The restitution coefficient can be shown as:

$$\varepsilon = v'/v \tag{1}$$

here the v and $v`$ are the velocities before and after the bounce. The impacting or bouncing velocity of the droplet is determined as:

$$v = (2gh)^{1/2} \tag{2}$$

The water droplet rebounds three times on surface-8 with restitution coefficient of 0.41, 0.17 and 0.14. However, when we impact water droplets on surface-1 to surface-7, the restitution coefficients are zero; the droplets stick to the surface due to the pinning of the contact line. In contrast, a stronger interfacial air layer prevents the droplet from penetrating into the interstices and getting pinned for surface-8[40].

For surface-8, the droplet flies vertically upwards until it is went up to the maximum height, then falls back onto the surface. The maximum height and the speed of the followed droplet are slightly lower than the previous impact due to the energy losses in the bouncing process. The droplet bounces again that leads to consecutive bouncing incidents at progressively decreased impact speed (Figure 3(h)). On the other hand, the loss of energy and the repeated bouncing are related to the wettability and the adhesion of the surface [41,42].

The restitution coefficient is decided according to the amount of the residual energy (E) which is shown as [39,43]:

$$E = E_1 - E_2 \tag{3}$$

Here, E_1 is the potential energy at initial state which is the same for these droplets, and E_2 is the energy loss (surface adsorption energy and transformation energy) during the impact process. The ratio of the air area on the surface help the droplet to rebound, the energy is less lost. In addition, the capillary pressure developing the trapped air is promoting the droplet rebound. The water droplet on surface-8 could be rebounded three times, and the water droplet on other surfaces could not be rebounded.

The $D(t)/D_0$ (time-dependent contact diameter of the droplet/the initial diameter of the droplet before impact) of surface-1 to surface-8 are shown in Figure 5(a). The maximum spreading diameter (D_{max}/D_0) is directly in connection with its final contact area and the contact time. This is an imperative parameter for controlling droplet deposition.

The $D(t)/D_0$ values are firstly increased to the maximum height, and then decreased. For surface-1 to surface-7 (Figure 5(a)–(g)), the $D(t)/D_0$ values are up and downs. However, the $D(t)/D_0$ value of surface-8 (Figure 4(h)) is decreased to zero due to the bouncing of the water droplet. The D_{max}/D_0 value and the $D(t)/D_0$ values with time were decreased from surface-1 to surface-8. This is due to the hydrophobic property of the surface.

The $H(t)/D_0$ variations of water droplet from surface-1 to surface-8 as a function of time are shown in Figure 5(b). The $H(t)/D_0$ values are decreased to the lowest datum firstly and then increased to a peak value. As time goes on, the values are damping, and the changes turned out to be less obviously. The rebound tendency of water droplets is evident with the higher hydrophobic property.

3.3 The surface morphology and hydrophobic property of the electrospinning films adding Al_2O_3

In order to continue increase the hydrophobic property of the electrospinning film, the nanoparticles of Al_2O_3 are added to enhance the surface roughness. The Al_2O_3 nanoparticles with 200 nm and 20 nm are added to the

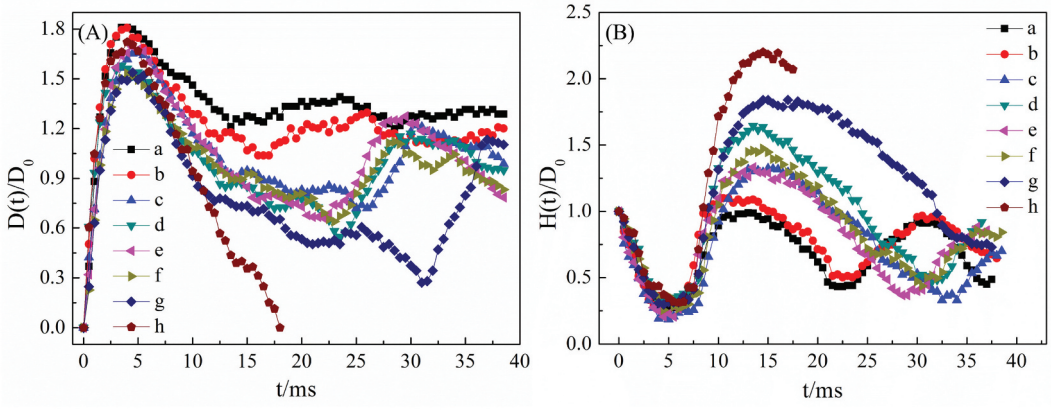

Figure 5. (a) The $D(t)/D_0$ of the droplet as a function of time. (b) The $H(t)/D_0$ variations of water droplet as a function of time. (a)-(h) surface-1 to surface-8, respectively.

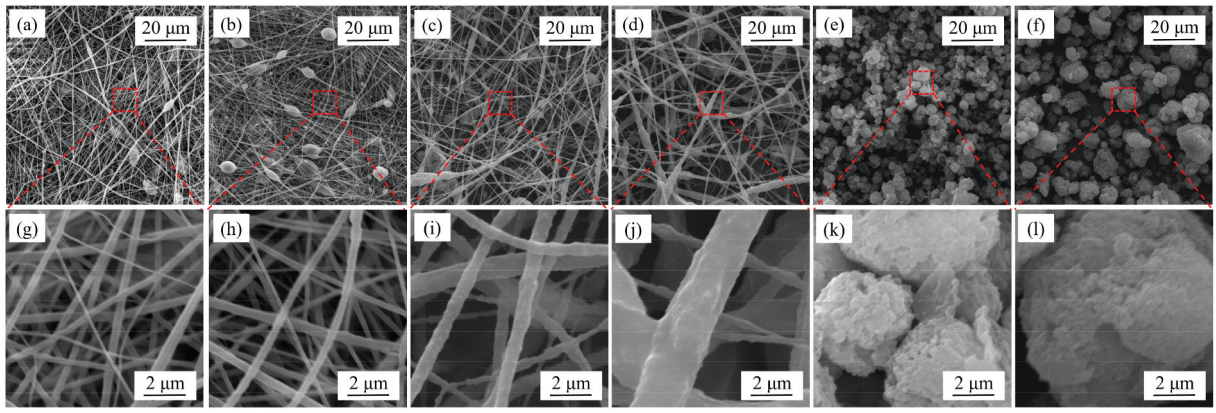

Figure 6. The SEM images of electrospinning films. (a)-(f) surface-9 to surface-14. (g)-(l) The drawing of partial enlargement of (a)-(f), respectively.

solution to fabricate the fabric. The surface morphologies of the electrospinning films are shown in Figure 6.

Figure 6 shows that the electrospinning film surface exhibits dense protrusion on its surface. Compared with surface-1 to surface-8, there are some rosary beads in the surface due to the aggregation of Al_2O_3. Dense and bumpy protrusion surface structure of surface-9 to surface-14 is believed as the main factor in rendering the electrospinning hydrophobic property. It can enhance the surface roughness which increase the surface hydrophobic property[30]. The water contact angles of the electrospinning films are shown in Figure 7. When added Al_2O_3, the hydrophobic property is increased which also enhance the surface roughness.

The water contact angles are increased when the ratio of DMF and THF from 5:5 to 9:1. The surface hydrophobic property is enhanced when added the nanoparticles. The water contact angle is 167.1° on surface-14. The morphologies of droplet impacting on surface-9 to surface-14 are exhibited in Figure 8.

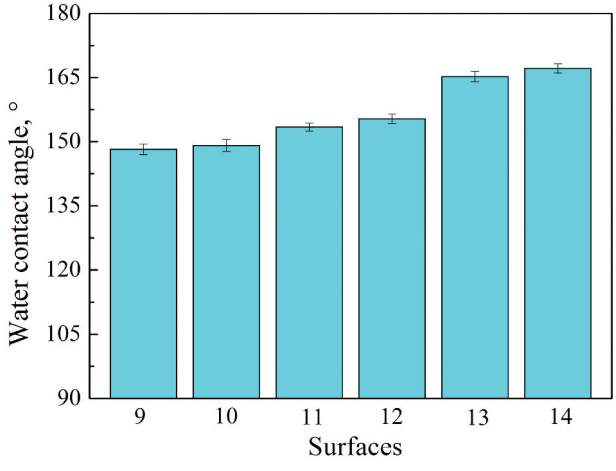

Figure 7. The water contact angles of surface-9 to surface-14.

As exhibited in Figure 8, a small droplet is splashing which break out at about 11 ms from surface-9 to surface-14. In addition, the large water droplet on the surface-9 to surface-12 is sticking to the surface all the time. On the other hand, the large water droplet is rebound five and six times when impact on surface-13 and surface-14, respectively. The splashing phenomenon is influenced by air compressibility and surface roughness. The roughness on a 1 nm scale is expected to further decrease the splash threshold impact velocity[44]. When added the Al_2O_3, the surface roughness is increased. The water droplet break into two parts. The hydrophobic property of the film added Al_2O_3 is more than that of the surfaces without Al_2O_3. The surface roughness is increased when added the Al_2O_3. The hierarchically porous and nanoparticle structures are prepared.

The POSS block copolymer could improve the hydrophobic property. In the electrospinning process, the porous structure film was formed through breath figure method. The fibers, Al_2O_3 nanoparticles and porous structure had micro/nano three-dimensional structure which can obvious enhance the surface hydrophobic property. The electrospinning fibers can be used for conventional applications, such as oil/water separation, self-cleaning materials. It opens up various possibilities for designing and developing a broad range of advanced multifunctional films.

3.4 The mechanical property of the electrospinning fibers

The electrospinning films should have a good mechanical property to its application. The mechanical behaviors of fiber films were closely to the intrinsic strength and bonding force of fibers[45]. The tensile properties of the typical electrospinning films are shown in Figure 9.

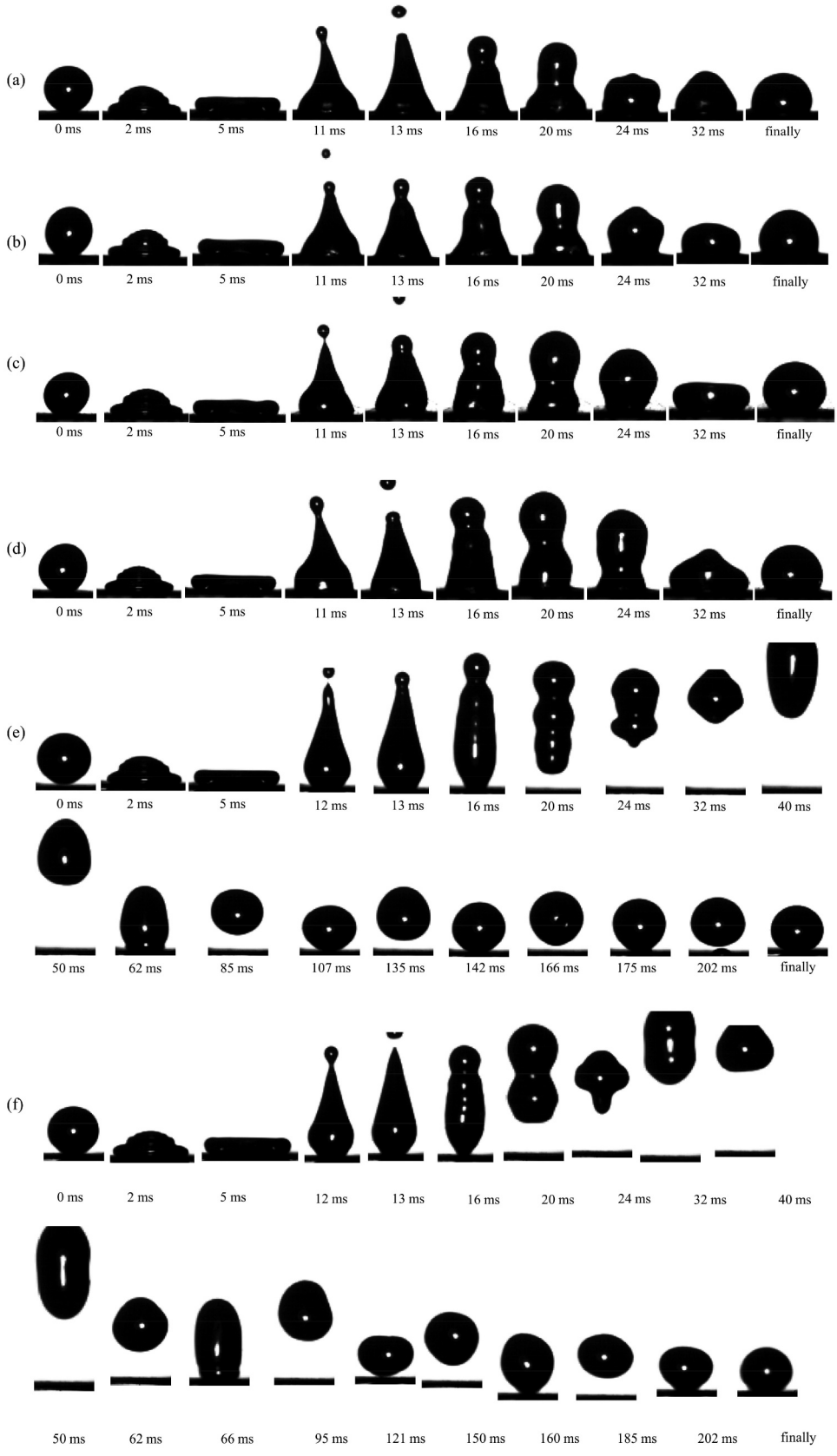

Figure 8. The morphologies of droplet impacting on different surfaces. (a)-(f) surface-9 to surface-14, respectively.

The increased of POSS block copolymer can cause the rise in mechanical strength and enhancement in tensile strain of the film, owing to the stronger mechanical properties of POSS block copolymer with high stress and low strain. The introduction of Al_2O_3 can improve the tensile strength of the films and the

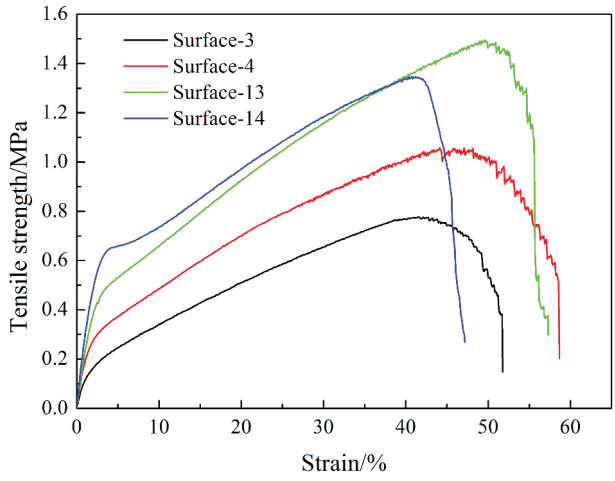

Figure 9. Stress-strain curves of the electrospinning fibers.

surface-13 and surface-14 had the larger tensile strength. It can be attributed to that appropriate amount of nanoparticles may contribute to the alignment of linear molecular chains in polymers[46]. The larger the particle size, the better the mechanical properties of the electrospinning films.

4. Conclusions

In this study, smooth fiber, porous fiber or hierarchically porous microspheres were prepared by the phase separation or breath figure method during electrospinning from polyhedral oligomeric silsesquioxanes (POSS) block copolymer, poly(vinylidene fluoride) (PVDF) or aluminium oxide (Al_2O_3). The influence of POSS-$(PTFEMA)_8$, the ratio of the solvents, the addition of Al_2O_3 on the surface morphology and microstructure were investigated. Porous fibers and porous microspheres were prepared by using the ratio of DMF:THF<5:5. The dynamic effect on the electrospinning films were reported. When the contact angle was 163°, the droplet bounces several times. In contrast, the droplet does not rebound and remains pinned when the contact angle was 140°. On the other hand, there is splashing phenomenon on the additional of Al_2O_3 electrospinning films. The hierarchically porous and nanoparticle structures were prepared, and the highest water contact angle of the electrospinning film adding Al_2O_3 with DMF: THF (1:9) was 167.1°. The increased of POSS block copolymer can cause the rise in mechanical property. Furthermore, the introduction of Al_2O_3 can improve the tensile strength of the films.

Acknowledgments

This work is supported by the Natural Science Foundation of Jiangsu Province (Grants No. BK20180588), the Fundamental Research Funds for the Central Universities (Grant JUSRP11702), Postgraduate Research &Practice Innovation Program of Jiangsu Province (Grant No. KYCX19_1853) and The Open Project Program of Key Laboratory of Eco-textiles, Ministry of Education, Jiangnan University (Grant No. KLET2002).

Disclosure statement

No potential conflict of interest was reported by the author(s).

Funding

This work was supported by the Fundamental Research Funds for the Central Universities [JUSRP11702]; Natural Science Foundation of Jiangsu Province [BK20180588]; Postgraduate Research &Practice Innovation Program of Jiangsu Province [KYCX19_1853]; The Open Project Program of Key Laboratory of Eco-textiles, Ministry of Education, Jiangnan University (No. KLET2002).

ORCID

Zhiguang Li http://orcid.org/0000-0002-4376-8365

References

[1] Lee DJ, Kim HM, Song YS, et al. Water droplet bouncing and superhydrophobicity induced by multiscale hierarchical nanostructures. ACS Nano. 2012;6(9):7656–7664.
[2] Ellinas K, Pujari SP, Dragatogiannis DA, et al. Plasma micro-nanotextured, scratch, water and hexadecane resistant, superhydrophobic, and superamphiphobic polymeric surfaces with perfluorinated monolayers. ACS Appl Mater Interfaces. 2014;6(9):6510–6524.
[3] Jafari R, Asadollahi S, Farzaneh M. Applications of plasma technology in development of superhydrophobic surfaces. Plasma Chem Plasma Process. 2013;33(1):177–200.
[4] Wu M, Ma B, Pan T, et al. Silver-nanoparticle-colored cotton fabrics with tunable colors and durable antibacterial and self-healing superhydrophobic properties. Adv Funct Mater. 2016;26(4):569–576.
[5] Xue C-H, Guo X-J, Ma J-Z, et al. Fabrication of robust and antifouling superhydrophobic surfaces via surface-initiated atom transfer radical polymerization. ACS Appl Mater Interfaces. 2015;7(15):8251–8259.
[6] Wang Z, Cong Y, Zhang B. Controllable wetting state high adhesion hydrophobic surface. RSC Adv. 2016;6(76):72815–72820.
[7] Chen L, Wang S, Yu Q, et al. A comprehensive review of electrospinning block copolymers. Soft Matter. 2019;15(12):2490–2510.

[8] Szewczyk PK, Stachewicz U. The impact of relative humidity on electrospun polymer fibers: from structural changes to fiber morphology. Adv Colloid Interface Sci. 2020;286: 102315.
[9] Fashandi H, Karimi M. Pore formation in polystyrene fiber by superimposing temperature and relative humidity of electrospinning atmosphere. Polymer. 2012;53 (25):5832–5849.
[10] Honarbakhsh S, Pourdeyhimi B. Scaffolds for drug delivery, part I: electrospun porous poly(lactic acid) and poly (lactic acid)/poly(ethylene oxide) hybrid scaffolds. J Mater Sci. 2011;46(9):2874–2881.
[11] Liu J, Chang M-J, Du H-L. Facile preparation of cross-linked porous poly(vinyl alcohol) nanofibers by electrospinning. Mater Lett. 2016;183:318–321.
[12] Cengiz U, Avci ZM, Erbil HY, et al. Superhydrophobic terpolymer nanofibers containing perfluoroethyl alkyl methacrylate by electrospinning. Appl Surf Sci. 2012;258(15):5815–5821.
[13] Zhao Y, Cao X, Jiang L. Bio-mimic multichannel microtubes by a facile method. J Am Chem Soc. 2007;129(4):764–765.
[14] Alayande SO, Dare EO, Msagati TAM, et al. Superhydrophobic and superoleophillic surface of porous beaded electrospun polystrene and polysytrene-zeolite fiber for crude oil-water separation. Phys Chem Earth Parts A/B/C. 2016;92:7–13.
[15] Crick CR, Parkin IP. Water droplet bouncing-a definition for superhydrophobic surfaces. Chem Comm. 2011;47 (44):12059–12061.
[16] Lu Y, Sathasivam S, Song J, et al. Water droplets bouncing on superhydrophobic soft porous materials. J. Mater. Chem. A. 2014;2(31):12177–12184.
[17] Rioboo R, Voué M, Vaillant A, et al. Drop impact on porous superhydrophobic polymer surfaces. Langmuir. 2008;24(24):14074–14077.
[18] Pham JT, Paven M, Wooh S, et al. Spontaneous jumping, bouncing and trampolining of hydrogel drops on a heated plate. Nat Commun. 2017;8(1):905.
[19] Koishi T, Yasuoka K, Zeng XC. Molecular dynamics simulation of water nanodroplet bounce back from flat and nanopillared surface. Langmuir. 2017;33 (39):10184–10192.
[20] Kim H, Lee C, Kim MH, et al. Drop impact characteristics and structure effects of hydrophobic surfaces with micro- and/or nanoscaled structures. Langmuir. 2012;28(30):11250–11257.
[21] Khojasteh D, Kazerooni M, Salarian S, et al. Droplet impact on superhydrophobic surfaces: a review of recent developments. J Ind Eng Chem. 2016;42:1–14.
[22] Wang M-J, Lin F-H, Hung Y-L, et al. Dynamic behaviors of droplet impact and spreading: water on five different substrates. Langmuir. 2009;25(12):6772–6780.
[23] Liu M, Zheng Y, Zhai J, et al. Bioinspired superantiwetting interfaces with special liquid–solid adhesion. Acc Chem Res. 2010;43(3):368–377.
[24] Liu M, Jiang L. Switchable adhesion on liquid/solid interfaces. Adv Funct Mater. 2010;20(21):3753–3764.
[25] Wang HX, Xue YH, Ding J, et al. Durable, self-healing superhydrophobic and superoleophobic surfaces from fluorinated-decyl polyhedral oligomeric silsesquioxane and hydrolyzed fluorinated alkyl silane. Angew Chem Int Edit. 2011;50(48):11433–11436.
[26] Gao Y, He C, Huang Y, et al. Novel water and oil repellent POSS-based organic/inorganic nanomaterial: preparation, characterization and application to cotton fabrics. Polymer. 2010;51(25):5997–6004.
[27] Wang P, Chung T-S. Recent advances in membrane distillation processes: membrane development, configuration design and application exploring. J Membrane Sci. 2015;474:39–56.
[28] An AK, Guo J, Lee E-J, et al. PDMS/PVDF hybrid electrospun membrane with superhydrophobic property and drop impact dynamics for dyeing wastewater treatment using membrane distillation. J Membrane Sci. 2017;525:57–67.
[29] Khraisheh M, AlMomani F, Al-Ghouti M. ElectrospunAl(2) O(3)hydrophobic functionalized membranes for heavy metal recovery using direct contact membrane distillation. Int J Energ Res. 2020; 45(6): 8151-8167.
[30] Damayanti NP. Preparation of superhydrophobic PET fabric from Al2O3-SiO2 hybrid: geometrical approach to create high contact angle surface from low contact angle materials. J Sol-Gel Sci Techn. 2010;56(1):47–52.
[31] Li Z, Zhang Z, Kong Q, et al. Adhesive and repulsive properties of water droplet impact on honeycomb surfaces through breath figure method. J Appl Polym Sci. 2017;134(47):n/a–n/a.
[32] Tan SH, Inai R, Kotaki M, et al. Systematic parameter study for ultra-fine fiber fabrication via electrospinning process. Polymer. 2005;46(16):6128–6134.
[33] Huang X, Gao J, Zheng N, et al. Influence of humidity and polymer additives on the morphology of hierarchically porous microspheres prepared from non-solvent assisted electrospraying. Colloids Surf A Physicochem Eng Asp. 2017;517:17–24.
[34] Gao JF, Wong JSP, Hu MJ, et al. Facile preparation of hierarchically porous polymer microspheres for superhydrophobic coating. Nanoscale. 2014;6(2):1056–1063.
[35] Liu J, Huang J, Wujcik EK, et al. Hydrophobic electrospun polyimide nanofibers for self-cleaning materials. Macromol Mater Eng. 2015;300(3):358–368.
[36] Theron SA, Zussman E, Yarin AL. Experimental investigation of the governing parameters in the electrospinning of polymer solutions. Polymer. 2004;45 (6):2017–2030.
[37] Huang X, Gao J, Li W, et al. Preparation of poly(ε-caprolactone) microspheres and fibers with controllable surface morphology. Mater Des. 2017;117:298–304.
[38] Long J, Fan P, Gong D, et al. Superhydrophobic surfaces fabricated by femtosecond laser with tunable water adhesion: from lotus leaf to rose petal. ACS Appl Mater Interfaces. 2015;7(18):9858–9865.
[39] Wu Y, Saito N, Nae FA, et al. Water droplets interaction with sSuper-hydrophobic surfaces. Surf Sci. 2006;600 (18):3710–3714.
[40] Wang Z, Lopez C, Hirsa A, et al. Impact dynamics and rebound of water droplets on superhydrophobic carbon nanotube arrays. Appl Phys Lett. 2007;91(2):023105.

[41] De Ruiter J, Lagraauw R, Van Den Ende D, et al. Wettability-independent bouncing on flat surfaces mediated by thin air films. Nat Phys. 2015;11 (1):48–53.
[42] Bartolo D, Boudaoud A, Narcy G, et al. Dynamics of non-newtonian droplets. Phys Rev Lett. 2007;99 (17):174502.
[43] Li Z, Kong Q, Ma X, et al. Dynamic effects and adhesion of water droplet impacts on hydrophobic surfaces: bouncing or sticking. Nanoscale. 2017;9(24):8249–8255.
[44] Mandre S, Brenner MP. The mechanism of a splash on a dry solid surface. J Fluid Mech. 2012;690:148–172.
[45] Tang X, Si Y, Ge J, et al. In situ polymerized superhydrophobic and superoleophilic nanofibrous membranes for gravity driven oil–water separation. Nanoscale. 2013;5 (23):11657–11664.
[46] Jiang Z, Tijing LD, Amarjargal A, et al. Removal of oil from water using magnetic bicomponent composite nanofibers fabricated by electrospinning. Compos Part B Eng. 2015;77:311–318.